Doping efficiency in freestanding silicon nanocrystals from the gas phase: Phosphorus incorporation and defect-induced compensation

A. R. Stegner,[1,*] R. N. Pereira,[1,2] R. Lechner,[1] K. Klein,[1] H. Wiggers,[3] M. Stutzmann,[1] and M. S. Brandt[1]
[1]*Walter Schottky Institut, Technische Universität München, Am Coulombwall 3, 85748 Garching, Germany*
[2]*Departamento de Física and I3N, Universidade de Aveiro, 3810-193 Aveiro, Portugal*
[3]*Institut für Verbrennung und Gasdynamik, Universität Duisburg-Essen, 47048 Duisburg, Germany*
(Received 16 June 2009; revised manuscript received 27 August 2009; published 23 October 2009)

Electron paramagnetic resonance (EPR) and secondary-ion mass spectroscopy have been used to quantitatively investigate the phosphorus doping of freestanding silicon nanocrystals (Si-NCs) in a wide range of diameters. It is found that both the atomic phosphorus incorporation efficiency of 100% and its segregation to the surface region during growth by our gas-phase method are independent of the nominal doping concentration and the Si-NC size. EPR data show that the concentration of electrically active substitutional P falls below the atomic P concentration by about 1 order of magnitude for Si-NC with diameters larger than 12 nm. Using a quantitative statistical model, charge compensation by Si dangling bonds is shown to be the reason for this difference. For smaller Si-NCs, a further strong drop of the concentration of paramagnetic donors is observed.

DOI: 10.1103/PhysRevB.80.165326 PACS number(s): 68.55.Ln, 61.46.Hk, 76.30.−v

I. INTRODUCTION

Owing to their interesting physical properties and the potential of cost-effective processing, semiconductor nanocrystals are currently breaking new ground in a wide field of applications ranging from solar cells, printable electronics, and thermoelectric power devices to efficient light emitters and devices for bioimaging.[1–8] For many applications it will be inevitable to tailor the properties of these emerging materials via controlled doping with impurity atoms. However, the doping of nanocrystals is, in general, quite distinct from their bulk counterparts.[9–12] Recent progress has been made in the understanding of doping mechanisms in II-VI semiconductor nanocrystals, which are grown using colloidal chemistry at relatively low temperatures.[13] There, the incorporation of impurities is governed by adsorption kinetics and can strongly depend on surface morphology and nanocrystal shape.[14] For silicon nanocrystals (Si-NCs) both electronic *p*- and *n*-type doping has been achieved with boron and phosphorus, respectively.[2,3,15–20] This includes Si-NCs embedded in amorphous oxides synthesized from solid-phase methods,[15,18,19] and freestanding Si-NCs from the gas phase.[2,3,16,20] P doping of Si-NCs grown from a liquid phase via coreduction of $SiCl_4$ and PCl_3 in 1,2-dimethoxyethane has also been reported.[17]

Freestanding Si-NCs grown from the gas phase are currently attracting a great deal of interest as a result of their advantageous properties with respect to the embedded silicon nanostructures studied more intensively until now. Gas-phase synthesis of freestanding Si-NCs relies on the decomposition of silane in a high-frequency plasma.[21–23] This scalable process has been optimized in the last years in terms of size dispersion, throughput and efficiency, so that sizable amounts of freestanding, mostly single-crystalline Si-NCs with selectable mean diameter in the range of 3–50 nm can be produced. The as-grown material can then directly be processed into semiconductor inks that can be used in printed electronic applications.[24] While quantum-size effects, which become prominent for the smallest Si-NCs, could be the basis for the development of band-gap tunable light emitters and photovoltaic cells that take advantage of efficient multiple exciton generation in Si-NCs,[25] in other applications that target, e.g., low-cost large-area production of electronic or thermoelectric devices, these effects are not necessarily beneficial. There, it is rather desirable to use larger NCs, where the surface-to-volume ratio and consequently also the number of unwanted surface defects is smaller and effects such as the misalignment of energy levels in interparticle transport or hindered doping can be avoided.

In recent investigations, it has been demonstrated that P and B can, in principle, be incorporated into Si-NCs during gas-phase synthesis by admixture of phosphine and diborane to the precursor gas.[2,16,20] Initial elemental-analysis experiments have shown that for P-doping concentrations below 4%, the incorporation efficiency of P atoms into the Si-NCs is nearly 100%.[2,20] However, for a narrow range of Si-NC diameters it was found that about 80–95 % of the P atoms incorporated segregate at the nanocrystal surface, depending on the specific growth method.[2,20] To act as an electronic donor, P has to be incorporated on substitutional sites of the Si-NCs core, which indeed has been demonstrated for the case of gas-phase synthesized Si-NCs by proof-of-principle magnetic-resonance experiments.[16,26]

Despite these recent developments, there is no quantitative understanding about the electronic doping efficiency of Si-NCs and only little is known about the incorporation efficiency and surface segregation of doping atoms during gas-phase synthesis and in their dependence on Si-NC size and nominal doping concentration. In this work, we quantitatively investigate the P doping of gas-phase Si-NCs in a wide range of diameters and doping levels. The size dependence of the electronic doping efficiency is studied using electron paramagnetic resonance (EPR), which allows the direct observation of donor-electron states, in conjunction with secondary-ion mass spectroscopy (SIMS), which is used to determine the atomic P concentrations. The paper is organized as follows: in the first part, we report EPR results on Si dangling-bond defects (Si-dbs) in Si-NCs and discuss the

surface density and spectral contributions from different Si-db defect species as a function of the Si-NC diameter and doping. Measuring the influence of thermal hydrogen desorption and annealing in hydrogen atmosphere on the Si-db density, we also directly demonstrate the importance of hydrogen for defect passivation in Si-NCs. In the second part of the paper, we discuss the P doping as a function of the Si-NC diameter. SIMS measurements of the as-grown material indicate an overall P incorporation efficiency of 100%, irrespective of the Si-NC size and the nominal doping concentration of up to 5×10^{20} cm^{-3}. However, after removal of the native oxide that forms after exposure of the Si-NCs to air, only about 5% of the initial P concentration is found in the remaining crystalline cores, which demonstrates a strong surface segregation of P during Si-NC growth. We find that the concentration of neutral, electrically active donors measured by low-temperature EPR, lies at least an order of magnitude below the atomic P concentration in the Si-NC core for all Si-NCs sizes. For Si-NCs larger than 12 nm in diameter, this discrepancy can be understood considering donor compensation by Si-dbs, for which we account for with a quantitative statistical model. For Si-NCs with diameters below 12 nm, the donor-electron concentration determined by EPR drops further by another 2 orders of magnitude with respect to the atomic P concentration. This observation is discussed in the last part of the paper in view of different physical effects such as donor confinement or charge transfer to the surface. However, our investigation demonstrates that a controlled P doping of Si-NCs with a diameter of $\gtrsim$12 nm can be performed successfully.

II. EXPERIMENTAL DETAILS

We have investigated phosphorus-doped and undoped Si-NCs, which were grown in a low-pressure microwave plasma reactor by microwave-induced decomposition of silane.[22] The resulting materials are powders of freestanding, spherical, and mostly single-crystalline Si-NCs.[22] Phosphorus doping of the Si-NCs was achieved by adding different amounts of phosphine from a dilute source containing 1% PH_3 in SiH_4 during growth. The nominal doping concentration, $[P]_{nom}$, is calculated as the fraction of phosphine in the total flow of precursor gases (SiH_4 and PH_3) multiplied by the atomic density of Si, $n_{Si}=5\times10^{22}$ cm^{-3}. The mean diameter of the Si-NCs can be selected between 3 and 50 nm by tuning the pressure of the process gases and the applied microwave power. A stable control of the gas flows in our reactor is only possible above a certain threshold value. This restricts the variation in the doping concentration for our smallest Si-NCs, where the lowest SiH_4 flows are required. There, $[P]_{nom}$ is fixed to 5×10^{20} cm^{-3}, corresponding to the PH_3 concentration in our doping source, as a further dilution by admixing additional SiH_4 would lead to larger Si-NC diameters.

In this work, we have investigated Si-NCs with a mean diameter between 4.3 and 47 nm as determined using the Brunauer-Emmett-Teller (BET) method.[27] The size distribution of our Si-NCs was determined for selected samples with particle mass spectroscopy and transmission electron microscopy (TEM) and shows a log-normal characteristic with a standard deviation that depends weakly on the mean diameter of the Si-NCs.[28] For the smallest Si-NCs investigated, the standard deviation of the diameter is $\sigma\approx1.3$ and increases to $\sigma\approx1.5$ for the Si-NCs with the largest diameters.[28] In the following, we define the Si-NC diameter d as the mean diameter measured by BET minus the average thickness of the native oxide shell of 1.4 ± 0.4 nm which was determined from TEM images of the Si-NCs. Therefore, the Si-NCs investigated have a mean core diameter between 1.5 and 44 nm.

EPR measurements were performed with a conventional continuous-wave *X*-band spectrometer and a TM_{110} cavity (Bruker). We used a lock-in amplifier for the detection of the EPR signal with a modulation of the magnetic field at 100 kHz. The sample temperature T was controlled using a He gas flow cryostat (Oxford). For EPR measurements, ≈1 mg of Si-NCs powder was filled into small Teflon tubes which were then placed in a conventional Suprasil quartz EPR sample holder. The mass of the samples was determined using a high-precision scale (Sartorius R200D). We estimate the overall error of the mass determination to be below 0.05 mg. Microwave power series were recorded with the different samples in order to make sure that the EPR signals investigated are free of saturation effects.

Annealing in vacuum was performed in a resistively heated radiant tube oven equipped with an evacuated ($\sim10^{-8}$ mbar) quartz tube. For annealing in hydrogen atmosphere, the quartz tube was filled with ultrapure 8 N hydrogen, which was removed only after the annealing, when the sample had reached room temperature.

For SIMS measurements, we prepared thin uniform films of densely packed Si-NCs with a thickness of $\approx$500 nm on top of Kapton Polyimide substrates which were coated by a 100 nm gold layer. The nanoparticle films were spin coated from a dispersion of Si-NCs in ethanol (6 wt %) which was prepared by a standard ball milling process.[29] SIMS profiles were measured with a ims4f-E6 mass spectrometer (Cameca) using Cs^+ (14.5 keV) as primary ions.

III. EXPERIMENTAL RESULTS AND DISCUSSION

A. Dangling-bond defects and H passivation

For the investigation of dangling-bond defects, we have performed EPR measurements at room temperature with different Si-NC powder samples. Figure 1 shows typical EPR spectra of doped and undoped Si-NCs with mean diameters of 1.5, 9.4, 42, and 44 nm (open circles). All spectra were normalized to the mass of the sample and show a broad asymmetric resonance located at $g\approx2.004-2.006$. The spectra of the Si-NCs with $d=9.4$ nm, $d=42$ nm, and $d=44$ nm can be decomposed by a computer simulation taking into account spectral contributions of (i) the powder pattern of a paramagnetic state with axial symmetry (dashed curves) and (ii) an isotropic signal (dotted curves). The best fit (black solid curves) is obtained for $g_\perp=2.0081(4)$ and $g_\parallel=2.0018(4)$ for the axially symmetric defect and $g=2.0055(5)$ for the isotropic resonance and leads to an excellent agreement with the experimental spectrum. We assign

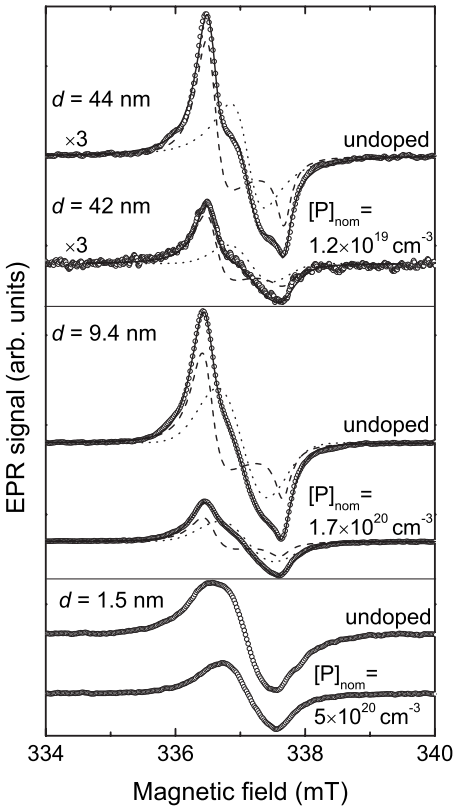

FIG. 1. Typical EPR spectra of doped and undoped Si-NCs measured at room temperature and normalized to the masses of the measured samples (open circles). The microwave frequency was 9.7345 GHz. The measured spectra can be decomposed by computer simulation using the powder pattern of a paramagnetic state with axial symmetry (dashed line) and an isotropic contribution (dotted line). The sums of these two contributions are shown as black solid lines. In the case of the Si-NCs with a diameter of 1.5 nm, the model described in the text cannot be used successfully to simulate the spectra. The spectra of the $d=42$ nm and $d=44$ nm samples were scaled up by a factor of 3.

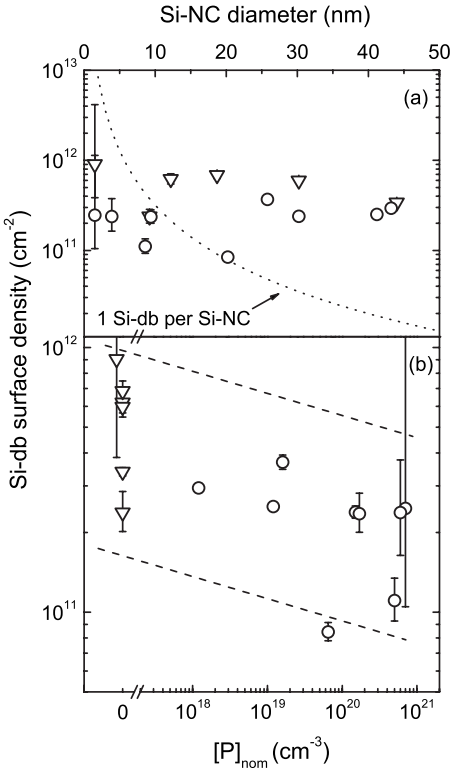

FIG. 2. In (a) the Si-db surface concentration, defined as the ratio between the amount of Si-db spins in the measured sample and the overall area of the Si/SiO_2 interface assuming an oxide thickness of 1.4 nm, is plotted as a function of the mean Si-NC diameter. The error bars reflect the uncertainty in the oxide thickness (± 0.4 nm). The dotted curve shows the Si-db concentration corresponding to one Si-db per Si-NC. In (b) the same data are shown as a function of the nominal doping concentration. The dashed lines are a guide to the eyes. Triangles and circles represent data from undoped and P-doped Si-NC samples, respectively. To avoid an overlap of the error bars in (b), the three data points at $[P]_{nom}=5\times10^{20}$ cm^{-3} were slightly displaced on the horizontal axis.

(i) to (111)-oriented trivalent Si atoms at the interface between the crystalline core of the Si-NCs and their native SiO_2 shell, so-called P_b centers.[30,31] The other signal at $g=2.0055$, which we denote as D signal, is typically observed in amorphous and polycrystalline Si as well as in Si-rich SiO_x and is assigned to threefold-coordinated Si in a randomly distorted environment.[32,33] Since we have no indications for significant amorphous contributions in the core of our Si-NCs, presumably also the D states are located close to the Si-NC surface. This is consistent with the observation of suboxide formation on H-terminated Si-NCs.[34] The peak-to-peak linewidths ΔB of 0.7 ± 0.1 mT for the D signal and $\Delta B_{\parallel}=0.3\pm0.1$ mT, $\Delta B_{\perp}=0.6\pm0.2$ mT for the P_b center compare well with the values typically reported in the literature.

The spectra of the $d=1.5$ nm samples are qualitatively different from the ones measured on larger Si-NCs. Due to the g value and the overall linewidth, we assign the signal to Si-dbs as well. However, the structure of the spectra is not resolved and can no longer clearly be decomposed with the numerical simulation described above. This could originate from a change in the principal g values of the axial spectrum due to a change in the interface between the Si-NC core and the surface oxide for Si-NC diameters below ≈10 nm, which is presumably induced by strain. We do not observe any systematic influence of P doping on the qualitative shape of the Si-db EPR spectra.

To assess the influence of Si-NC size and doping on the Si-db defect concentration, we determine the density of neutral, paramagnetic Si-dbs by double numerical integration of the Si-db related EPR resonances and comparison of the obtained intensity with a 2,2-diphenyl-1-picrylhydrazyl reference sample containing a known number of paramagnetic states. In Fig. 2(a) the Si-db surface density is plotted as a function of the Si-NC diameter. The measured EPR data was normalized to the overall Si/SiO_2-interface area of the different samples calculated on the basis of the BET surface. The error bars reflect the uncertainty of this normalization originating from the uncertainty of the oxide thickness (±0.4 nm). Results for doped and undoped samples are shown as circles and triangles, respectively. The dotted curve indicates the defect concentration that corresponds to an av-

erage of one Si-db per NC. As can be seen in Fig. 2(a), Si-NCs with diameters below 10 nm contain less than one defect on average, which is an important prerequisite for the use of Si-NCs in various applications. For undoped samples we do not observe a significant dependence on the Si-NC size and we find an average surface concentration of $\approx 5 \times 10^{11}$ cm^{-3} which is comparable to Si-db concentrations around 10^{12} cm^{-3} typically found at bulk Si/SiO_2 interfaces.[35]

For doped Si-NCs we do not find a size dependence of the Si-db concentration as well. However, a trend that is already reflected in the spectra shown in Fig. 1 is a decrease in the density of Si-db defects upon doping with P. To give a more quantitative overview of this effect in Fig. 2(b), we plot the data shown in Fig. 2(a) as a function of the nominal doping concentration. Although the scatter of the data is quite large, a decrease in the defect density with increasing nominal P-doping concentration can be observed as a general trend. Quantitatively, the average measured Si-db concentration changes approximately by a factor of 2 when going from undoped material to Si-NCs with $[P]_{nom}=5\times10^{20}$ cm^{-3}. This phenomenon can, in principle, be explained by two effects: (i) as proposed in previous studies of Si-NCs embedded in amorphous SiO_2,[20,36] P atoms might decrease the defect density by reducing strain at the Si/SiO_2 interface. (ii) Since Si-dbs are amphoteric defects, with an electronic level located close to midgap, they can capture donor electrons to form ionized P^+ donors and negatively charged diamagnetic Si-db states, which no longer contribute to the Si-db EPR signal.[37] In contrast to (i) this charge compensation does not reduce the actual number of Si-db defects in the Si-NCs. As shall be discussed below, from analysis of EPR data obtained for P donor electrons, we conclude that compensation (ii) should be the dominant mechanism leading to the observed decrease in the Si-db density with P doping. The weakness of the observed compensation effect already suggests that either the doping efficiency or the compensation mechanism are very different from the situation in the bulk.

The scatter of the Si-db defect density of the undoped Si-NC samples most likely originates from the different growth conditions, in particular, different amounts of hydrogen that were incorporated during growth of the different Si-NC samples. To directly demonstrate the role of H in the passivation of Si-db defects in Si-NCs, we compare EPR spectra of as-grown Si-NCs ($d=25.8$ nm) with EPR spectra measured after annealing in vacuum at 450 °C for 30 min, and after annealing at 410 °C for 30 min in ultrapure hydrogen at a pressure of 1 atm. Such a comparison is shown in Fig. 3 together with the numerical fits that were obtained in the same way as for the spectra in Fig. 1. Spectrum (a), which was measured on the as-grown sample, has the typical shape as described for Fig. 1, resulting from spectral contributions from P_b centers and D states, which are again represented by dashed and dotted lines, respectively. After annealing in vacuum at 450 °C [curve (b)], the shape of the EPR defect signal remains almost unchanged and the intensities of both spectral contributions is increased by a factor of 4.0 ± 0.1. The observed increase in Si dangling-bond defects upon heating can directly be correlated with the effusion of hydrogen from the sample and is also reflected in a quenching of Si-H vibrational bands in infrared-absorption spectra measured after annealing.[38] Annealing the as-grown sample in molecular hydrogen decreases the amount of Si-dbs, as can be seen in Fig. 3(c). The intensity of the EPR signal is clearly reduced with respect to the spectrum of the as-grown sample and the shape of the resonance has become more symmetric. The decomposition of the spectrum reveals that the intensity of the D signal remains almost unchanged with respect to the as-grown sample while the intensity of the P_b is reduced by a factor of 0.6. These changes can be explained by a passivation of Si dangling bonds with hydrogen during the annealing, which, for the applied temperature and pressure, is more effective for P_b centers than for D states. This result is consistent with the recently reported, efficient passivation of P_b centers using a very similar treatment for solid-phase-grown Si-NCs embedded in SiO_2 matrices.[39]

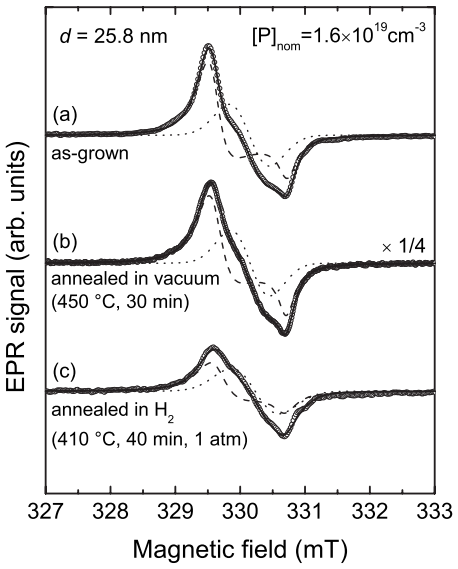

FIG. 3. Room-temperature EPR spectra of P-doped Si-NCs ($[P]_{nom}=1.6\times10^{19}$ cm^{-3}) with a mean diameter of 25.8 nm. Curve (a) shows the spectrum of the as-grown sample, spectrum (b) was recorded after annealing in vacuum at 450 °C for 30 min, and curve (c) was measured after annealing an as-grown sample in pure H_2 at 410 °C and at a pressure of 1 atm for 30 min. The spectra were normalized to the masses of the measured samples. Curve (b) was scaled down by a factor of 4. As in Fig. 1 the spectra are shown together with their numerical fits.

B. Phosphorus donors

For the investigation of P doping in Si-NCs, we employ two complementary experimental techniques. We use SIMS to determine the atomic density of P in an ensemble of Si-NCs and low-temperature EPR in order to directly measure the number of electrically active P that were incorporated on substitutional lattice sites in our Si-NCs.

In Fig. 4(a), typical SIMS profiles of Si-NCs with a mean diameter of $d=9.4$ nm and $[P]_{nom}=1.7\times10^{20}$ cm^{-3} are shown, plotting the measured P concentration, [P], as a function of the depth. The solid curve shows the profile of a film that was processed from as-grown Si-NCs. The measured

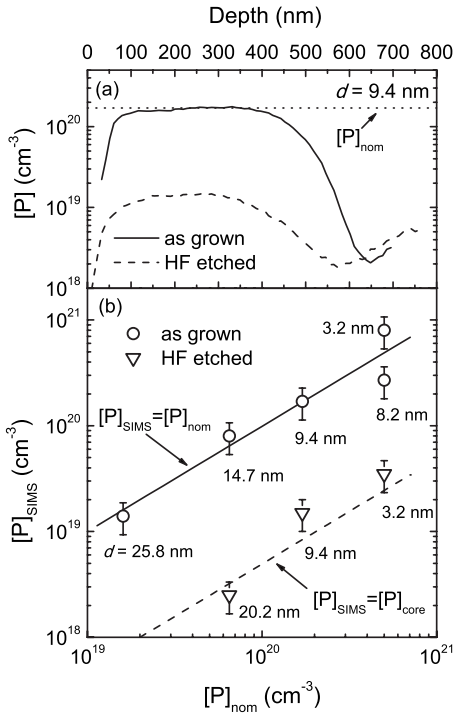

FIG. 4. (a) SIMS profiles of thin films of Si-NCs with a mean diameter of 9.4 nm and $[P]_{nom}=1.7\times10^{20}$ cm^{-3}. The solid curve shows the profile of the as-deposited film, the dashed curve was measured after immersing the Si-NC film in 5 wt %. hydrofluoric acid. (b) Measured P concentration, $[P]_{SIMS}$, extracted from the plateau regions of the SIMS profiles, versus $[P]_{nom}$ before (circles) and after etching in hydrofluoric acid (triangles). The data points are labeled with the mean Si-NC diameter of the measured sample. The solid line correspond to $[P]_{SIMS}=[P]_{nom}$ and the dashed line shows $[P]_{SIMS}=[P]_{nom}/20$.

atomic P concentration in the region of the plateau between 100 and 400 nm is in very good agreement with $[P]_{nom}$, which is indicated by the dotted line. This means that the phosphorus offered during gas-phase growth was incorporated into the Si-NCs with practically 100% efficiency. The dashed curve shows a SIMS profile that was measured on the same sample after an etching step, where the film was immersed in 5 wt % hydrofluoric acid (HF) for 15 s and subsequently washed in deionized water. This etching step leads to an efficient removal of the native oxide shells of the as-grown Si-NCs throughout the entire film, and predominantly a hydrogen termination of the Si-NC surfaces is attained.[16] The SIMS profile of the etched Si-NCs shows a P concentration that is reduced by a factor of 12 from the concentration in the as-deposited film to 1.4×10^{19} cm^{-3} in the region of the plateau. In addition, the plateau region is narrower and the edges of the plateau are washed out in the case of the profile of the etched film, which could be explained by an etching-induced reduction in the structural quality of the Si-NC film.

The strong decrease in the measured P concentration upon etching can only be explained if most of the P resides in the native oxide shell of the Si-NCs. To obtain a more comprehensive picture of this phenomenon, we recorded SIMS profiles of films of various Si-NC samples with different doping concentration and diameter, before and after HF etching. The data points in Fig. 4(b), represent $[P]_{SIMS}$, the atomic P concentration in the plateau region of the different SIMS profiles before (circles) and after (triangles) removal of the native oxide shells. The data points are labeled with the mean Si-NC diameter of the different samples. The upper dashed line corresponds to $[P]_{SIMS}=[P]_{nom}$, i.e., a P incorporation efficiency of 100%. The lower dashed line represents $[P]_{SIMS}=[P]_{nom}/20$, which corresponds to the average reduction in $[P]_{SIMS}$ after the HF etching step and is hereafter denoted as $[P]_{core}$. As can be seen, our data can be well explained if we assume that ≈95% of the P is located in the native oxide shells of the Si-NCs. We explain this observation by a segregation of P atoms to the Si-NC surface during growth and subsequent oxidation of the highly doped shell. This behavior is known from molecular-beam epitaxy growth of Si:P (Ref. 40) and has recently also been reported for Si-NCs grown from the gas phase in a VHF plasma.[20] There, the authors employ inductively coupled plasma atomic emission spectroscopy for the elemental analysis of their Si-NC samples and find a minus 80% change in the P concentration after removal of the oxide for Si-NCs with an average diameter of 3.6 nm, which were synthesized at temperatures below 600 °C. For the Si-NCs investigated in our study, the growth temperature exceeds 1000 °C for a few milliseconds. The higher growth temperature, allowing an enhanced P diffusion, could explain the somewhat stronger surface segregation in our Si-NCs as compared to Ref. 20.

As the atomic density of P atoms in an ensemble of Si-NCs does not necessarily correspond to the density of P that act as electrically active donors, we employ low-temperature EPR measurements, where the concentration of substitutional donors can directly be determined. Figure 5(a) shows the EPR spectra of two Si-NC samples with mean NC diameters of 42 and 43 nm, and different nominal doping concentrations, measured at $T=20$ K. Besides the broad Si-db resonance, which is also observed at room temperature and is now partially saturated, both spectra show additional features. For the Si-NCs with $[P]_{nom}=1.3\times10^{18}$ cm^{-3}, a resonance centered at $g=1.998$ and two further lines denoted hf(^{31}P) are observed, which are symmetrically split to the high- and low-field sides of the $g=1.998$ resonance, with a total separation of ≈4.1 mT.[16] The splitting of the latter pair of lines originates from the Fermi-contact hyperfine interaction of P donor electrons in the ground state and the ^{31}P donor nuclei which carry a nuclear spin $I=1/2$. A hyperfine splitting of 4.2 mT and a central g value of 1.9985 constitute the characteristic EPR fingerprint of substitutional, isolated P in crystalline Si (c-Si).[41,42] The central resonance at $g=1.998$ originates from exchange coupled, more closely spaced, substitutional P atoms or from free electrons. In c-Si such a signal is characteristic for intermediate and high P concentrations.[42–45] In the second spectrum in Fig. 5(a), which was measured on Si-NCs with a ten times higher doping concentration ($[P]_{nom}=1.2\times10^{19}$ cm^{-3}), the hf(^{31}P) lines disappear whereas the line at $g=1.998$ increases in intensity.

The EPR spectra shown in Fig. 5(b) were recorded with two Si-NC samples of the same nominal doping concentration of 5×10^{20} cm^{-3} but different mean particle diameters

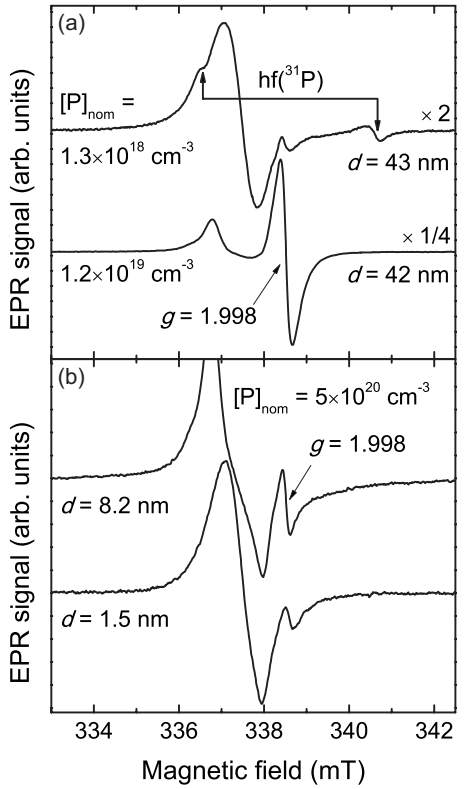

FIG. 5. (a) EPR spectra of Si-NCs with a mean diameter of 42 and 43 nm, and nominal doping concentrations of $[P]_{nom}=1.2\times10^{19}$ cm^{-3} and $[P]_{nom}=1.3\times10^{18}$ cm^{-3}, respectively. (b) EPR spectra of doped Si-NCs with mean diameters of 8.2 and 1.5 nm. All spectra were measured under the same experimental conditions at $T=20$ K and their intensity was normalized to the sample mass.

of 8.2 and 1.5 nm. Again, besides the broad defect related resonance at $g\approx2.006$, the P-related line at $g=1.998$ is observed. The observation of this characteristic resonance shows the successful substitutional incorporation of P, also in small Si-NCs with diameters below 10 nm.[16] However, compared to the high nominal doping concentration, the intensity of the P signal is rather low, and approximately three times weaker for the 1.5 nm sample than for the 8.2 nm sample. These results suggest a decrease in the overall doping efficiency with decreasing Si-NC size.

To assess this effect in more detail, we analyze the spectra quantitatively. However, for bulk Si, a Curie-temperature dependence of the magnetic susceptibility of localized magnetic moments scaling as T^{-1} is only expected for donor concentrations below 3×10^{18} cm^{-3}.[43,45] Exceeding this value, the Pauli paramagnetism from degenerate donor electrons starts to diminish the temperature dependence of the EPR signal intensity. This no longer allows for an easy determination of the absolute amount of donor electrons via a comparison of the measured signal intensity with a known spin standard, as this would require to assume a constant Fermi level throughout the whole ensemble of Si-NCs measured and to know its concrete position.[44] To determine the donor density from the EPR signal intensity, we therefore need to measure the temperature dependence of the intensity of the $g=1.998$ EPR resonance to ascertain a Curie behavior.

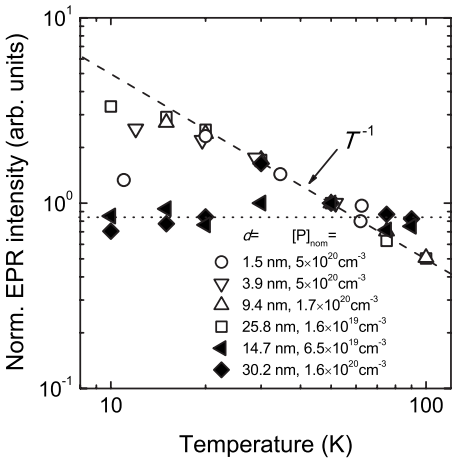

FIG. 6. Temperature dependence of the EPR signal intensity of the $g=1.998$ resonance for different Si-NC samples with a diameter d and a nominal doping concentration $[P]_{nom}$ shown in a double-logarithmic plot. The data was normalized so that all samples show the same signal intensity at $T=50$ K. The dashed line represents a T^{-1} Curie behavior. The dotted line indicates a temperature-independent Pauli behavior.

The results of such measurements, where we calculated the intensity of the $g=1.998$ signal by numerical double integration of the resonance line, are shown in a double-logarithmic plot in Fig. 6 for the samples with the highest $[P]_{nom}$. While the two samples with mean NC diameters of 14.7 and 30.2 nm and nominal doping concentrations of 6.5×10^{19} cm^{-3} and 1.6×10^{20} cm^{-3}, respectively, show a temperature-independent Pauli behavior over the whole temperature range investigated, all other samples show a T^{-1} behavior for >20 K. For temperatures <20 K, we observe a modified Curie paramagnetism,[46] which has also been observed in bulk c-Si:P.[43] For the evaluation of the absolute amount of paramagnetic donor-electron spins in the samples that show a Curie-temperature behavior, we use spectra that were recorded at $T=20$ K, where the maximum signal intensity in the Curie regime is obtained.

Based on $[P]_{EPR}$, the concentration of donor electrons that contribute to the EPR signal at $g=1.998$, we define the doping efficiency in our Si-NC samples as $[P]_{EPR}/[P]_{nom}$. Here, $[P]_{EPR}$ is obtained from the intensity of the EPR signal, however, in principle, also the width of the donor-related EPR line can be used as a measure for the P-doping concentration in Si. A correlation between the linewidth and the P-doping concentration in c-Si has been established for a wide range of doping concentrations.[42–45] However, these studies were performed using single-crystalline bulk samples, where charge compensation and surface effects were negligible. In Si-NC ensembles, the donor-related resonance line is an ensemble signal composed of contributions from separated, partially compensated NCs with different doping concentrations due to statistical fluctuations of the number of donors per NC. Moreover, in contrast to bulk samples, most of the donors are located relatively near to the surface, which can strongly influence the spin-relaxation time and consequently the EPR linewidth.[47] Thus, in Si-NC ensembles, the EPR linewidth is a much less reliable quantity for the estimation

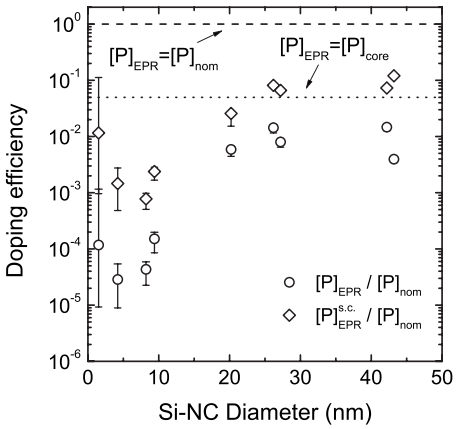

FIG. 7. P-doping efficiency as determined from the spin density of the $g=1.998$ peak at $T=20$ K as a function of the Si-NC diameter. The circles show the measured $[P]_{EPR}$ normalized to $[P]_{nom}$ and the diamonds show the same data after correcting for charge compensation of donors by Si-dbs ($[P]^{s.c.}_{EPR}$), assuming the model described in the text. The dashed and dotted lines show the cases $[P]_{EPR}=[P]_{nom}$ and $[P]_{EPR}=[P]_{core}$, respectively.

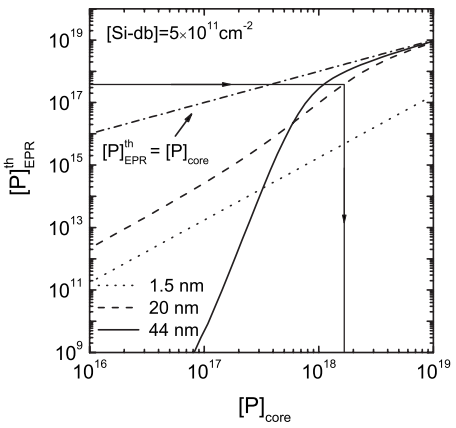

FIG. 8. $[P]^{th}_{EPR}$ as a function of $[P]_{core}$ for $d=44$ nm, $d=20$ nm, and $d=1.5$ nm as calculated using the compensation model based on Eq. (1) described in the text. The dash-dotted line displays the limit $[P]^{th}_{EPR}=[P]_{core}$.

of the donor concentration than in bulk crystals. In order to illustrate the influence of the size on the doping efficiency, we plot $[P]_{EPR}/[P]_{nom}$ for the Si-NC samples that show a Curie behavior as a function of the mean Si-NC diameter in Fig. 7 (open circles). The error bars again result from the uncertainty of the oxide thickness (± 0.4 nm). If every P atom in the crystalline core of the Si-NC samples contributed to the EPR donor-electron signal (i.e., $[P]_{EPR}=[P]_{core}$), we would expect a plateau for $[P]_{EPR}/[P]_{nom}$ at 5×10^{-2} (dotted line) in accordance with the SIMS results. However, all measured data points indicated by the circles in Fig. 7 fall well below this value.

As already mentioned above, the Si-dbs in our Si-NC samples should lead to charge compensation of P donors,[37] which might explain this discrepancy. Using the information about the defect concentration obtained from room-temperature EPR measurements, we can estimate the effect of charge compensation by Si-dbs quantitatively. For this, we have to take into account that, unlike in large bulk crystals, in NC ensembles the particulate character of the sample leads to a partial separation of donors and defects. To address this effect, we set up a simple statistical compensation model which is based on the following assumptions: (i) within a single Si-NC, donors and Si-dbs compensate each other one-to-one and interparticle compensation does not occur due to the Si-NC oxide shell. (ii) The number of P donors and Si-dbs per particle follow binomial probability distributions. (iii) An average Si-db surface concentration of $[\text{Si-db}]=5\times10^{11}$ cm^{-2} is assumed for all Si-NC samples. This value corresponds to the average Si-db concentration measured for undoped Si-NC samples (cf. Fig. 2). (iv) In order to contribute to the observed $g=1.998$ resonance, a Si-NC has to have a minimum number, N_{min}, of two P atoms ($N_{min}=2$). Si-NCs with one P atom can only contribute to the hyperfine split EPR signal of isolated donors.[42] Under these assumptions, the average number of spins per Si-NC contributing to the $g=1.998$ resonance can be calculated by

$$N_{spins}=\sum_{j=N_{min}}^{\infty}\sum_{i=0}^{j-1}[(j-i)W^{N_{Si}}_{p_P}(j)W^{A_{Si}}_{p_{db}}(i)]. \quad (1)$$

Here, $W^{N_{Si}}_{p_P}(j)$ is the binomial probability to find j phosphorus atoms in a particle with $N_{Si}=(\pi/6)d^3n_{Si}$ silicon atoms, where the probability for any lattice site to be occupied by P is simply given by $p_P=[P]_{core}/n_{Si}$. An analogous definition holds for $W^{A_{Si}}_{p_{db}}$, where A_{Si} is the Si-NC surface area and p_{db} is the probability to find one Si-db per unit area. Thus, N_{spins} effectively is a function of $[P]_{core}$, d, and [Si-db]. Using Eq. (1) we define the donor-electron concentration that should theoretically be detected by EPR, taking into account compensation, as $[P]^{th}_{EPR}=(N_{spins}/N_{Si})\times n_{Si}$, where N_{spins} is calculated for a Si-NC that has the mean diameter of the Si-NC ensemble and contains N_{Si} atoms. We neglect the Si-NC size distribution in our powder samples for the simulation.

In Fig. 8 we plot $[P]^{th}_{EPR}$ as a function of $[P]_{core}$ for $d=1.5$, 20, and 44 nm. The dash-dotted line displays the limit $[P]^{th}_{EPR}=[P]_{core}$, i.e., the case when all P donors are uncompensated. For very high doping concentrations $[P]^{th}_{EPR}$ approaches this limiting case asymptotically for all NC diameters, as the number of Si-dbs in a NC becomes negligible compared to the amount of P donors. When the average number of Si-dbs and P donors per particle are comparable, the compensation behavior strongly depends on the Si-NC size. For the 44 nm Si-NCs we observe a rather sharp onset of $[P]^{th}_{EPR}$ for 10^{17} cm$^{-3}<[P]_{core}<10^{18}$ cm^{-3}. In this region, the average number of P atoms per Si-NC increases from 4 to 45 and crosses the average number of 32 Si-dbs for Si-NCs with $d=44$ nm. In general, compensation becomes less effective as the Si-NC size decreases due to a stronger separation of P and Si-dbs. This trend is reflected by the much flatter slope of $[P]^{th}_{EPR}$ calculated for $d=20$ nm. For our smallest NCs ($d=1.5$ nm), the calculation results in a straight line (dotted curve) which is shifted to much lower $[P]^{th}_{EPR}$ with respect to the 20 nm curve. The reason for this behavior is that for the smallest Si-NCs the probability distribution of the number of P atoms per Si-NC peaks at zero

also for high $[P]_{core}$ (up to 10^{19} cm^{-3}), i.e., the probability to find no P atoms in a Si-NC is the highest. As only Si-NCs that contain more than one P atom ($N_{min}=2$) contribute to $[P]_{EPR}$, this leads to a strong downward shift of $[P]^{th}_{EPR}$ for $d=1.5$ nm in Fig. 8. In fact, this statistical effect dominantly determines $[P]^{th}_{EPR}$ for Si-NC diameters below ≈ 3 nm as the separation effect becomes so strong in this size regime (i.e., the probability to find a P donor and a Si-db in the same Si-NC becomes so low) that charge compensation is negligible under the assumptions made for our model.

The solid horizontal arrow in Fig. 8 indicates $[P]^{th}_{EPR}=3.8\times10^{17}$ cm^{-3}, which corresponds to the measured concentration of donor electrons, $[P]_{EPR}$, for one of our samples with $d=20$ nm. Evaluating $[P]_{core}$ at the intersection of this line and the theoretical compensation curve (dashed), we can now recursively determine the atomic density of P in the Si-NC core that is needed to explain the measured EPR signal intensity $[P]_{EPR}$. We denote this statistically corrected concentration as $[P]^{s.c.}_{EPR}$. The results of this statistical correction for all our samples are shown as diamonds in Fig. 7. For diameters larger than 12 nm, the data points form a plateau at $[P]^{s.c.}_{EPR}/[P]_{nom}\approx 0.5-1\times10^{-1}$. The good alignment with the dashed line which indicates $[P]_{core}$, determined by SIMS, shows that donor compensation by Si-dbs alone is sufficient to explain the above-mentioned discrepancy between $[P]_{core}$ and $[P]_{EPR}$. As a consequence, we can conclude that nearly all of the P atoms incorporated in the Si-NCs and not consumed by the surface oxide are located on substitutional sites for Si-NC diameters larger than 12 nm.

In Fig. 7, we observe a sharp drop of $[P]_{EPR}/[P]_{nom}$ for $d<12$ nm by more than 2 orders of magnitude. As can be seen from the small value of $[P]^{s.c.}_{EPR}$ at the same diameter, compensation alone cannot account for this decrease in the doping efficiency, if the assumptions made for our compensation model also hold for Si-NCs with $d<12$ nm. A reduced doping efficiency is also reflected by the temperature dependence of the EPR signal shown in Fig. 6. In spite of the highest $[P]_{nom}$ in our smallest Si-NCs, a Pauli behavior is not observed for these samples. A straight forward explanation for the strong drop of the doping efficiency for Si-NCs with $d<12$ nm could be the increase in the number of interface sites, where P does not act has a donor, with respect to internal (bulklike) sites for smaller NCs. The relative increase in interface sites increases with decreasing nanocrystal size as $1/d$ and could be further enhanced if P locates preferentially close to the interface. However, this effect should lead to a continuous decrease in the donor-electron concentration with the decreasing size (as $1/d$), which is not observed experimentally. As can be seen in Fig. 7, for diameters in the range of 2–10 nm, where this effect would be very strong, we do not observe a significant decrease in the donor-electron concentration.

Another fact worth noticing is that if compensation is ineffective for the small Si-NCs and the probability to find Si-NCs containing no or only a single P atom is higher than the probability of having more than one P, as our compensation model suggests, it is puzzling that we do not observe the characteristic hyperfine pair of neutral, isolated P donors in the EPR spectra of the smallest Si-NC samples in Fig. 5. One possible explanation for the absence of the hyperfine lines in the EPR spectra of the small Si-NCs could be the dependence of the hyperfine splitting on the NC size.[26] In conjunction with the size distribution of our Si-NC ensembles, this effect leads to a broadening of the EPR hyperfine peaks which could strongly impede their detection due to sensitivity limitations. In a recent study, we used electrically detected magnetic resonance (EDMR) under illumination to determine the magnitude of the broadening effect for our Si-NC samples.[26] This technique has a much larger sensitivity than conventional EPR for electrically active impurities, however, it cannot be used to quantify the number of donors in our samples as outlined in Ref. 16. For the smallest Si-NCs studied using EDMR ($d=6$ nm), we find a peak-to-peak linewidth of ≈ 2.5 mT.[26] For a typical EPR detection sensitivity of at least 10^{11} spins per 0.1 mT linewidth,[48] $\gtrsim 6\times10^{13}$ isolated donor spins should be sufficient to observe the characteristic hyperfine signal taking into account the two hyperfine split resonance lines of isolated P. All samples investigated with $d<12$ nm should have $[P]_{core}\approx 1\times10^{19}$ cm^{-3}, which corresponds to $\approx 10^{15}$ isolated donors in a $d=6$ nm sample with a typical mass of 1 mg used in our investigation, which is somewhat above the sensitivity limit of an optimized EPR setup. Nevertheless, the characteristic hyperfine signal is not observed in our experiments, which points to an additional loss mechanism of donor electrons.

In view of all the results obtained for small Si-NCs, two effects could possibly be responsible for the small values of $[P]_{EPR}/[P]_{nom}$ for $d<12$ nm: (a) in contrast to assumption (i) in our statistical model, compensation of donors across Si-NC boundaries could become significant for small Si-NCs. This might be due to the enhanced surface-to-volume ratio and an enhanced tunneling probability of donor electrons through the oxide barrier due to quantum confinement of the donor-electron wave function. (b) P donor electrons could be captured by nonparamagnetic trap states at the Si-NC surface,[49,50] which cannot be detected by EPR but lead to an additional depletion of P donors. The formation of these surface trap states might be a function of the Si-NC size. Donor electrons could as well be lost due to chemical reactions at the Si-NC surface, where a P-doped Si-NC could act as reducing agent.[9]

IV. CONCLUSION

We have quantitatively investigated the doping efficiency and the interrelationship of intrinsic Si-db states and P doping in freestanding Si-NCs grown from the gas phase. Si-db states of the P_b and D type are found at densities comparable to bulk Si/SiO_2 interfaces and no significant dependence on the NC size is observed. Hydrogen was shown to play an important role in Si-db passivation in Si-NCs. Annealing of the as-grown material to temperatures beyond 400 °C leads to a strong increase in the Si-db concentration due to hydrogen desorption. Phosphorus is incorporated into freestanding Si-NCs grown from the gas phase with an efficiency close to 100% independently of the Si-NC size. However, the predominant part of the donors ($\approx 95\%$) segregates to the surface region of the Si-NCs during growth. Such segregation is

also independent of the Si-NC size and nominal doping level. For all Si-NC diameters, the donor-electron concentration measured with EPR is at least one order of magnitude smaller than the atomic P density in the Si-NC cores. For Si-NCs larger than 12 nm, this effect is quantitatively explained on the basis of charge compensation by Si-db defects alone. For smaller Si-NCs with high $[P]_{nom}$, the measured donor-electron concentration drops down sharply to values three orders of magnitude below the atomic P concentration. We propose that this effect results from internanocrystal compensation or electron capture at surface-related states. Further investigations will be necessary to clarify the situation for Si-NCs with diameters below 12 nm. From our study we conclude that the use of Si-NCs with diameters larger than 12 nm is advantageous for application in electronic devices where a well-defined and controlled electronic doping with P is required.

ACKNOWLEDGMENTS

The authors are grateful to Marco Hoeb for support with the annealing experiments in hydrogen atmosphere. The work at Walter Schottky Institut has been supported by the EU (PSYNANO) and the DFG (Grant No. SFB 631, C3), at University Duisburg-Essen by the DFG (Grant No. GK 1240). The project was additionally supported by Evonik Degussa S2B Nanotronics, the state of North Rhine-Westfalia and the EU as well as by CRUP-DAAD via an "Acção Integrada Luso-Alemã."

*stegner@wsi.tum.de

[1] I. Gur, N. A. Fromer, M. L. Geier, and A. P. Alivisatos, Science **310**, 462 (2005).
[2] R. Lechner, A. R. Stegner, R. N. Pereira, R. Dietmueller, M. S. Brandt, A. Ebbers, M. Trocha, H. Wiggers, and M. Stutzmann, J. Appl. Phys. **104**, 053701 (2008).
[3] R. Lechner, H. Wiggers, A. Ebbers, J. Steiger, M. S. Brandt, and M. Stutzmann, Phys. Status Solidi (RRL) **1**, 262 (2007).
[4] C. Liu, Z. C. Holman, and U. R. Kortshagen, Nano Lett. **9**, 449 (2009).
[5] Y. Kanemitsu, S. Okamoto, M. Otobe, and S. Oda, Phys. Rev. B **55**, R7375 (1997).
[6] K. Nishiguchi, X. Zhao, and S. Oda, J. Appl. Phys. **92**, 2748 (2002).
[7] X. Michalet, F. F. Pinaud, L. A. Bentolila, J. M. Tsay, S. Doose, J. J. Li, G. Sundaresan, A. M. Wu, S. S. Gambhir, and S. Weiss, Science **307**, 538 (2005).
[8] D. Jurbergs, E. Rogojina, L. Mangolini, and U. Kortshagen, Appl. Phys. Lett. **88**, 233116 (2006).
[9] D. J. Norris, A. L. Efros, and S. C. Erwin, Science **319**, 1776 (2008).
[10] D. J. Norris, N. Yao, F. T. Charnock, and T. A. Kennedy, Nano Lett. **1**, 3 (2001).
[11] F. V. Mikulec, M. Kuno, M. Bennati, D. A. Hall, R. G. Griffin, and M. G. Bawendi, J. Am. Chem. Soc. **122**, 2532 (2000).
[12] S. B. Orlinskii, J. Schmidt, P. G. Baranov, D. M. Hofmann, C. de Mello Donegá, and A. Meijerink, Phys. Rev. Lett. **92**, 047603 (2004).
[13] Y. Yin and A. P. Alivisatos, Nature (London) **437**, 664 (2005).
[14] S. C. Erwin, L. Zu, M. I. Haftel, A. L. Efros, T. A. Kennedy, and D. J. Norris, Nature (London) **436**, 91 (2005).
[15] M. Fujii, Y. Yamaguchi, Y. Takase, K. Ninomiya, and S. Hayashi, Appl. Phys. Lett. **87**, 211919 (2005).
[16] A. R. Stegner, R. N. Pereira, K. Klein, R. Lechner, R. Dietmueller, M. S. Brandt, M. Stutzmann, and H. Wiggers, Phys. Rev. Lett. **100**, 026803 (2008).
[17] R. K. Baldwin, J. Zou, K. A. Pettigrew, G. J. Yeagle, R. D. Britt, and S. M. Kauzlarich, Chem. Commun. (Cambridge) **2006**, 658.
[18] M. Fujii, A. Mimura, S. Hayashi, Y. Yamamoto, and K. Murakami, Phys. Rev. Lett. **89**, 206805 (2002).
[19] K. Sumida, K. Ninomiya, M. Fujii, K. Fujio, S. Hayashi, M. Kodama, and H. Ohta, J. Appl. Phys. **101**, 033504 (2007).
[20] X. D. Pi, R. Gresback, R. W. Liptak, S. A. Campbell, and U. Kortshagen, Appl. Phys. Lett. **92**, 123102 (2008).
[21] M. Otobe, T. Kanai, T. Ifuku, H. Yajima, and S. Oda, J. Non-Cryst. Solids **198-200**, 875 (1996).
[22] J. Knipping, H. Wiggers, B. Rellinghaus, P. Roth, D. Konjhodzic, and C. Meier, J. Nanosci. Nanotechnol. **4**, 1039 (2004).
[23] L. Mangolini, E. Thimsen, and U. Kortshagen, Nano Lett. **5**, 655 (2005).
[24] L. Mangolini and U. Kortshagen, Adv. Mater. **19**, 2513 (2007).
[25] M. C. Beard, K. P. Knutsen, P. Yu, J. M. Luther, Q. Song, W. K. Metzger, R. J. Ellingson, and A. J. Nozik, Nano Lett. **7**, 2506 (2007).
[26] R. N. Pereira, A. R. Stegner, T. Andlauer, K. Klein, H. Wiggers, M. S. Brandt, and M. Stutzmann, Phys. Rev. B **79**, 161304(R) (2009).
[27] S. Brunauer, P. H. Emmett, and E. Teller, J. Am. Chem. Soc. **60**, 309 (1938).
[28] B. Giesen, H. Wiggers, A. Kowalik, and P. Roth, J. Nanopart. Res. **7**, 29 (2005).
[29] M. Gjukic, R. Lechner, and M. Stutzmann, German Patent Application No. 102005056446 (26 November 2006).
[30] E. Poindexter, P. Caplan, B. Deal, and R. Razouk, J. Appl. Phys. **52**, 879 (1981).
[31] A. Stesmans and V. V. Afanas'ev, J. Appl. Phys. **83**, 2449 (1998), and references therein.
[32] M. Stutzmann and D. K. Biegelsen, Phys. Rev. B **40**, 9834 (1989).
[33] E. San Andrés, A. del Prado, I. Mártil, G. González, F. L. Martínez, D. Bravo, F. J. López, and M. Fernández, Vacuum **67**, 525 (2002).
[34] X. D. Pi, L. Mangolini, S. A. Campbell, and U. Kortshagen, Phys. Rev. B **75**, 085423 (2007).
[35] N. M. Johnson, W. B. Jackson, and M. D. Moyer, Phys. Rev. B **31**, 1194 (1985).
[36] M. Fujii, A. Mimura, and K. Yamamoto, Appl. Phys. Lett. **75**, 184 (1999).
[37] P. M. Lenahan and J. F. Conley, J. Vac. Sci. Technol. B **16**, 2134 (1998).

[38] A. R. Stegner, R. N. Pereira, K. Klein, H. Wiggers, M. S. Brandt, and M. Stutzmann, Physica B **401-402**, 541 (2007).
[39] S. Godefroo, M. Hayne, M. Jivanescu, A. Stesmans, M. Zacharias, O. I. Lebedev, G. van Tendeloo, and V. V. Moshchalkov, Nat. Nanotechnol. **3**, 174 (2008).
[40] J. F. Nützel and G. Abstreiter, Phys. Rev. B **53**, 13551 (1996).
[41] G. Feher, Phys. Rev. **114**, 1219 (1959).
[42] P. R. Cullis and J. R. Marko, Phys. Rev. B **11**, 4184 (1975).
[43] H. Ue and S. Maekawa, Phys. Rev. B **3**, 4232 (1971).
[44] J. D. Quirt and J. R. Marko, Phys. Rev. B **5**, 1716 (1972).
[45] J. D. Quirt and J. R. Marko, Phys. Rev. B **7**, 3842 (1973).
[46] E. Sonder and H. C. Schweinler, Phys. Rev. **117**, 1216 (1960).
[47] R. de Sousa, Phys. Rev. B **76**, 245306 (2007).
[48] D. C. Maier, Bruker Rep. **144**, 13 (1997).
[49] P. Zhang, E. Tevaarwerk, B. Park, D. E. Savage, G. K. Celler, I. Knezevic, P. G. Evans, M. A. Eriksson, and M. G. Lagally, Nature (London) **439**, 703 (2006).
[50] K. C. Lin, O. W. Holland, L. C. Feldman, and H. H. Weitering, Appl. Phys. Lett. **72**, 2313 (1998).